Title

Defect Chemistry as a Crystal Structure Design Parameter: Intrinsic Point Defects and Ga Substitution in InMnO3

Journal

Chemistry of Materials, 29(6)

ISSN

0897-4756

Authors

Griffin, Sinéad M
Reidulff, Mari
Selbach, Sverre M
et al.

Publication Date

2017-03-28

DOI

10.1021/acs.chemmater.6b04207

Peer reviewed

CHEMISTRY OF MATERIALS

Review

pubs.acs.org/cm

Defect Chemistry as a Crystal Structure Design Parameter: Intrinsic Point Defects and Ga Substitution in $InMnO_3$

Sinéad M. Griffin,*[,†,‡] Mari Reiduff,[‖] Sverre M. Selbach,*[,‖] and Nicola A. Spaldin*[,§]

[†]Molecular Foundry, Lawrence Berkeley National Laboratory, Berkeley, California 94720, United States

[‡]Department of Physics, UC Berkeley, Berkeley, California 96720, United States

[‖]Department of Materials Science and Engineering, NTNU Norwegian University of Science and Technology, NO-7491 Trondheim, Norway

[§]Materials Theory, ETH Zurich, Wolfgang-Pauli-Strasse 27, CH-8093 Zurich, Switzerland

ABSTRACT: The effect of defect chemistry on the polar and nonpolar phases of hexagonal $InMnO_3$ is investigated using first-principles density functional calculations. Our motivation is to show how point defects and substitutional atoms can modify the delicate balance between ferroelectric and nonferroelectric phases in a complex multiferroic oxide. By analyzing the distinct In corrugation patterns of the competing phases, we find that oxygen interstitials, indium vacancies and indium−oxygen vacancy pairs favor the polar $P6_3cm$ phase, which is also the ground state of stoichiometric $InMnO_3$. The polar $P3c1$ phase is stabilized by oxygen vacancies, while Ga substitution on the Mn site destabilize the ferroelectric phases and favor instead the nonpolar $P\bar{3}c$ or $P6_3/mmc$ structures. In addition to the structure, the electrical properties are also strongly dependent on the defect chemistry, ranging from metallic to large band gap insulating. The implications of the strong influence of vacancies, interstitials and substitutions on the ferroelectric and electronic properties are discussed with respect to synthesis and applications.

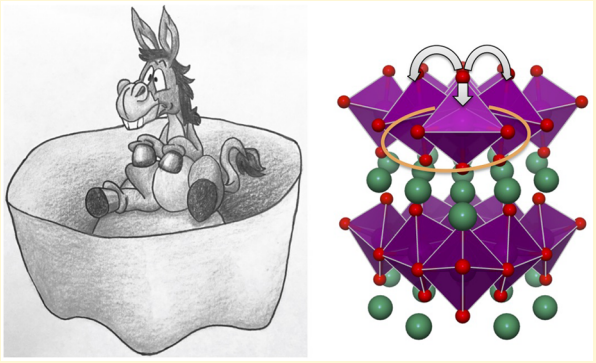

INTRODUCTION

The search for multiferroic materials, with their multiple coexisting ferroic orders, has been a hotbed of research activity in recent decades[1−5] and has led to the identification of new mechanisms for ferroelectricity that are compatible with the coexistence of magnetism.[6] The so-called *improper geometric ferroelectricity* identified in the rare-earth hexagonal manganites, $RMnO_3$ (R = Sc, Y, Dy, Ho, Er, Tm, Yb, Lu, In), is of particular interest and has stimulated research in topics as diverse as high-temperature multiferroism,[7] nanodevices,[8,9] and testing of early universe theories.[10]

The high-symmetry $P6_3/mmc$ prototype structure of the hexagonal manganites consists of layers of corner-sharing Mn−O trigonal bipyramids separated by layers of Y, In, or small rare-earth ions (Figure 1a). The $P6_3cm$ ferroelectric structure has a tripled unit cell which is reached through a trimerizing tilting of the trigonal bipyramids at one of six equivalent angles around the z axis (labeled ϕ = 0°, 60°, etc.) (Figure 1b).[11−14] The tilting is accompanied by staggered "up−up−down" z displacements of the R cations that cause the nonzero polarization. Analysis of the structure and symmetry indicates that an equivalent trimerizing tilting at the exactly intermediate angles of ϕ = 30°, 90°, etc., accompanied by "up−none−down" rare-earth z displacements yields the nonpolar $P\bar{3}c$ structure shown in Figure 1d.[13] Trimerization tiltings at arbitrary ($\phi \neq 0$ or 30°) angles are accompanied by noncanceling z displacements and result in the lower-symmetry ferroelectric $P3c1$ space group (Figure 1c), which is a subgroup of both $P6_3cm$ and $P\bar{3}c$.[15]

While the ferroelectric $P6_3cm$ structure is well established to be the ground state for most members of the series, the behavior of $InMnO_3$ has been controversial. The first flux-grown samples were reported from X-ray diffraction measurements to have the high-symmetry $P6_3/mmc$ structure,[16] whereas polycrystalline samples annealed at 1000 °C in an evacuated sealed quartz tube indicated a unit-cell tripling that was interpreted in terms of the polar $P6_3cm$ structure.[17] The polar state was supported by measurements of polarization−electric field hysteresis loops that were interpreted in terms of a ferroelectric polarization;[18] subsequent dielectric measurements on high quality ceramics interpreted similar loops as dielectric loss behavior and concluded an absence of polarization.[19] A study of Ga-substituted $In(Mn,Ga)O_3$[20] obtained a good refinement of the X-ray data within the $P6_3cm$ symmetry group and obtained refined atomic positions consistent with a substantial ferroelectric polarization but failed to observe signatures of ferroelectricity in dielectric, phonon, second-

Special Issue: Computational Design of Functional Materials

Received: October 3, 2016
Revised: February 11, 2017
Published: February 13, 2017

DOI: 10.1021/acs.chemmater.6b04207
Chem. Mater. 2017, 29, 2425−2434

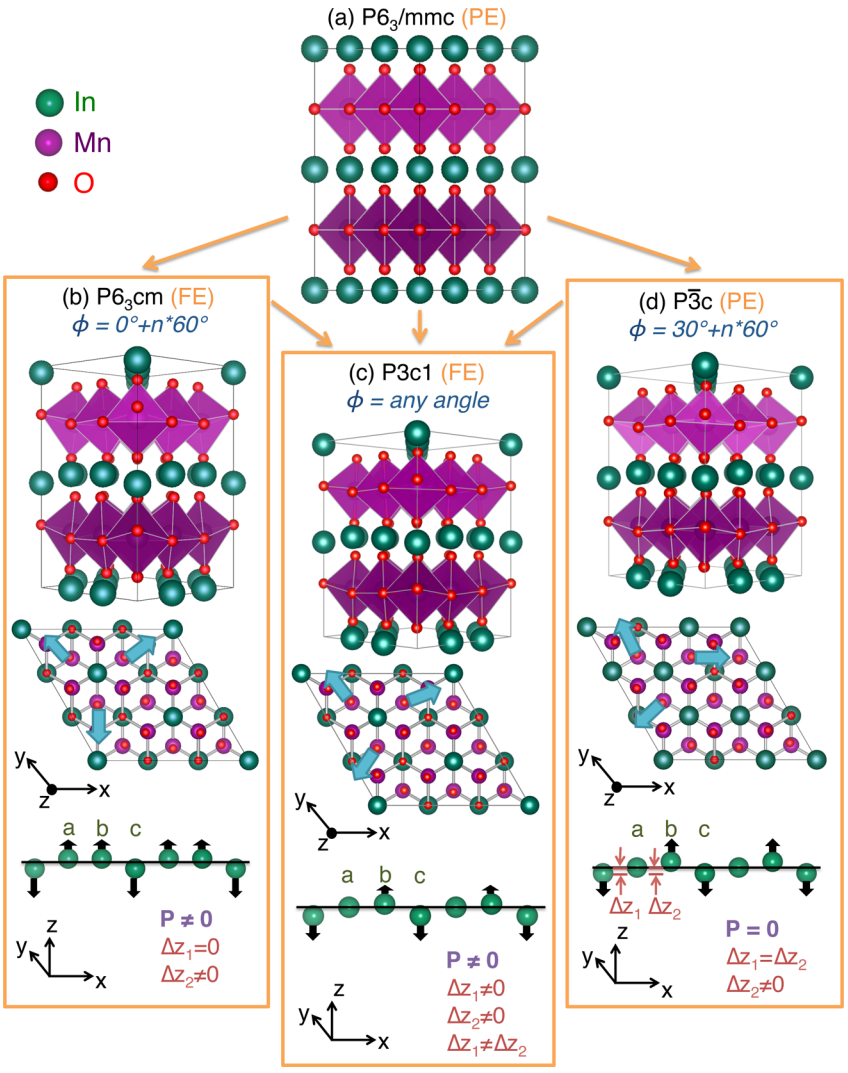

Figure 1. (a) High-symmetry paraelectric (PE) $P6_3/mmc$ structure of $InMnO_3$. Note the absence of trimerization. (b–d) Low symmetry structures of $InMnO_3$. (a) Ferroelectric (FE) $P6_3cm$ structure with $\phi = 60° + n60°$, (b) ferroelectric $P3c1$ structure with a general tilt angle ϕ, and (d) nonpolar $P\bar{3}c$ structure with $\phi = 30° + n60°$. In b–d the middle panel illustrates with blue arrows the pattern of tilting of the MnO_5 trigonal bipyramids, and the lower panel shows the In displacements along the z axis ("up–up–down", intermediate, and "up–down–none" for $P6_3cm$, $P3c1$, and $P\bar{3}c$, respectively).

harmonic-generation, and differential scanning calorimetry measurements. This inconsistency was somewhat resolved by a subsequent analysis of X-ray data for $InMnO_3$, which found equally good refinements using either $P6_3cm$ or $P\bar{3}c$ symmetries.[14] Their comprehensive study combining piezoresponse force microscopy (PFM) and second harmonic generation (SHG) also failed to find evidence of polarization; accompanying first-principles calculations based on density functional theory found a very small energy difference between the centrosymmetric $P\bar{3}c$ and ferroelectric $P6_3cm$ structures.[14] Recently, Bekheet et al.[21] prepared single crystals of $InMnO_3$ with PbF_2 flux to avoid the Bi impurities reported for single crystals grown in a Bi_2O_3 flux[22,23] and concluded that the ambient structure is $P6_3cm$ based on single crystal X-ray diffraction, SHG, and PFM.

A breakthrough in understanding was made when it was shown that the details of the sample preparation affect the resulting ferroelectric properties.[23] Using transmission electron microscopy (TEM) and high-angle annular dark-field scanning (HAADF) TEM, ferroelectricity was found in slowly cooled samples, whereas fast cooling in a furnace was shown to favor the centrosymmetric phase. A follow-up study combining first-principles calculations with HAADF-TEM[15] demonstrated that all three possible phases discussed in the symmetry analysis above could be obtained simultaneously in a single sample and showed that their coexistence is due to extremely shallow energy barriers separating the states. We note that, while distinguishing between the $P6_3cm$, $P\bar{3}c$, and $P3c1$ space groups is difficult using XRD, particularly when they coexist in a single sample, HAADF-TEM experiments image the In displacements and can thus detect the local structural details corresponding to the different symmetries.[15] In addition, it was shown that substitution of Ga on the Mn site could be used to tune between the various phases. It now seems likely that ideal, stoichiometric $InMnO_3$ has the $P6_3cm$ ferroelectric ground state, with the nonpolar $P\bar{3}c$ phase, as well as the low-symmetry ferroelectric $P3c1$ and possibly even the high-symmetry paraelectric reference $P6_3/mmc$ structures, accessible by modifying the defect concentration or overall stoichiometry.

DOI: 10.1021/acs.chemmater.6b04207
Chem. Mater. 2017, 29, 2425–2434

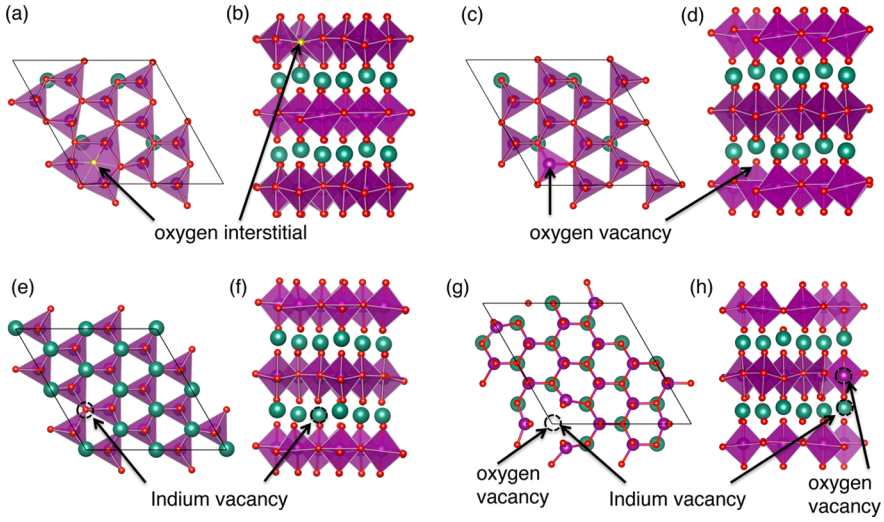

Figure 2. Calculated lowest-energy structures for interstitial and vacancy defects in $InMnO_3$. (a and b) Calculated lowest-energy structure containing one oxygen interstitial per 24 formula units. The oxygen interstitial lies in the Mn−O plane, and the structure retains the $P6_3cm$-type symmetry, with "up−down−down" In displacements, of the stoichiometric material. (c and d) Calculated structure for one oxygen vacancy per 24 formula units. The oxygen vacancy is at the apex of a trigonal bipyramid, and the In displacements reveal the resulting $P3c1$-type structure. The calculated lowest-energy structures for $InMnO_3$ containing indium vacancies are shown in e and f and for indium−oxygen vacancy complexes in g and h. Both structures show an "up−down−down" pattern of In displacements indicating $P6_3cm$-type structures; in the vacancy complex case the In and O vacancies are directly above each other with the same x and y coordinates.

These combined findings point to an essential role of point defects in determining the structural ground state and, hence, the ferroelectric properties of $InMnO_3$. While the point defect chemistry of perovskite oxides has been studied extensively due to their importance in electronic and energy technology applications and has been shown to strongly influence functionality, particularly in the context of strained thin films,[24−27] far less is known about the role of point defects in hexagonal $RMnO_3$. We anticipate strong effects, since $RMnO_3$ have already been shown to tolerate significant oxygen deficiency down to $3 - \delta = 2.75$,[28] excess oxygen up to $\delta = 0.35$,[29,30] and R^{3+} deficiency down to $1 - x = 0.72$.[31] The possibility of In deficiency is even more likely due to the relatively high volatility of In at typical temperatures for single-crystal growth or sintering of polycrystals, with a vapor pressure over solid In at 950 °C, for example, of 5.4×10^{-5} atm.[32]

In this work we use first-principles electronic structure calculations based on density functional theory to perform a comprehensive study of the role of various defects in determining the ground state polar or nonpolar structure of $InMnO_3$, as well as the resulting properties. Specifically, we calculate the influence of oxygen vacancies and interstitials, indium vacancies, indium−oxygen vacancy pairs, and Ga substitution on the Mn site. We find that, because of the energetic proximity of multiple competing ground states in $InMnO_3$, the coupling between structure, defect chemistry, and functionality is even stronger than in the case of the perovskite oxides, where it is also of tremendous current interest in the context of strained thin films.[24−27] Finally we discuss the enticing possibility of switching between the polar and nonpolar phases through reversible modifications of the defect profile.

COMPUTATIONAL DETAILS

We performed density functional calculations using the projector augmented wave (PAW) method as implemented in the Vienna Ab initio Simulation Package (VASP).[33,34] In(4d, 5s, 5p), Mn(3p, 3d, 4s), Ga(3d, 4s, 4p), and O(2s, 2p) electrons were treated as valence electrons, and their wave functions expanded in plane waves to an energy cutoff of 550 eV. The Brillouin zone was sampled using Gamma-centered k-point grids of $4 \times 4 \times 2$ and $2 \times 2 \times 2$ for 30- and 120-atom unit cells, respectively. The magnetic ordering was initialized to be collinear with alternating planes of "up−up−down" and "down−up−down" ordering;[35] spin−orbit coupling was not included. Since our defect concentrations are high, corresponding to typical experimental concentrations, we performed full structural relaxations of the internal coordinates and the cell shape and size until the Hellmann−Feynman forces were below 1 meV/Å and the stresses were below 0.01 kbar for each defect chemistry studied. We considered neutral defect cells since charged defect cells are unexpected for finite defect concentrations in this low band gap transition metal oxide.

Previous ab initio studies[14,15] found that the ground-state energetics are sensitive to the choice of exchange-correlation functional. For spin-polarized Perdew−Burke−Ernzerhof functionals (PBE),[36] for example, a nonpolar ground state is slightly favored for stoichiometric $InMnO_3$, whereas the spin-polarized PBE plus Hubbard U (GGA+U) method yields a ferroelectric ground state, in agreement with the likely experimental situation. For our calculations we used the PBE functional in its form that is modified for solids (PBEsol),[37] as this typically gives excellent agreement with experiment for bond lengths and lattice parameters, and added an effective Hubbard U term, $U_{eff} = U - J = 4$ eV, in keeping with previous work on $InMnO_3$ and other hexagonal manganites.[38] With these settings we found the $P6_3cm$ phase to be only 4 meV per formula unit lower in energy than the $P\bar{3}c$, consistent with the previously calculated near degeneracy of the two phases.[14,15] Both structures were found to be insulating with a calculated band gap of 1.21 eV for the $P\bar{3}c$ phase and 1.16 eV for the $P6_3cm$ phase.

The inclusion of interstitials, substitutions, and vacancies lowers the symmetry from the ideal cases discussed above, making a direct comparison of the role of defects on the

DOI: 10.1021/acs.chemmater.6b04207
Chem. Mater. 2017, 29, 2425−2434

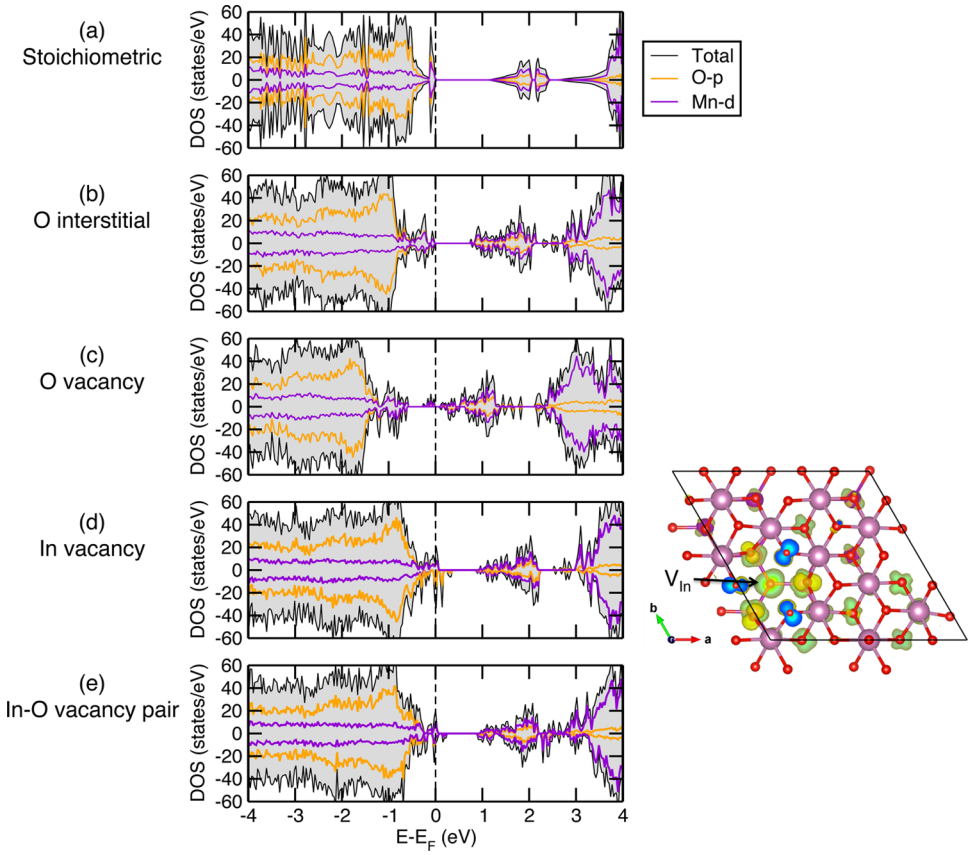

Figure 3. Calculated densities of states for (a) stoichiometric $InMnO_3$ and (b–e) the lowest-energy structures shown in Figure 2 containing the following defects (each per 24 unit cells of $InMnO_3$): (b) one oxygen interstitial, (c) one oxygen vacancy, (d) one indium vacancy, and (e) one In–O vacancy pair. The gray shading shows the total density of states, and the purple and orange lines show the Mn-d and O-p states. The Fermi energy is set to 0 eV and marked by the dashed line. Alongside d, the In vacancy density of states, we show the partial charge density in a region around the Fermi energy, which is localized in the Mn-d and O-p orbitals adjacent to the vacancy site.

structural stability of the competing phases nontrivial. To assign our defective structures to one of the four space groups, we analyze the z displacements of the In ions in the region of the unit cell furthest from the location of the defects. In the case of the prototype paraelectric $P6_3/mmc$ structure, all In ions in the same plane have the same z value. For the lower-symmetry structures we label three consecutive In ions along the x direction as a, b, and c, with z coordinates z_a, z_b, and z_c. We then define $\Delta z_1 = z_a - z_b$ and $\Delta z_2 = z_b - z_c$. The ideal $P6_3cm$ structure is then indicated by one zero and one nonzero Δz value, $P\bar{3}c1$ by nonzero and equal Δz_1 and Δz_2, and $P3c1$ by nonzero and unequal values. In our defective systems we refer to the corresponding structures as "$P6_3/mmc$-type", "$P6_3cm$-type", etc. In borderline cases we take a tolerance threshold on the difference between Δ_z values of 0.002 Å.

RESULTS

Oxygen Defects. To study the effects of oxygen vacancies and oxygen interstitials, we introduced single point defects into 2 × 2 × 1 supercells, containing 24 formula units, of the nonpolar $P\bar{3}c1$-type and polar $P6_3cm$-type structures. These supercells provide defect separations of ∼12 Å, which are sufficiently large for the interaction of periodic images to be neglected.[39] We then relaxed the atomic positions and cell parameters. The magnetism was initialized to the collinear antiferromagnetic order described above and remained in that state.[35]

The formation of oxygen interstitials can be expressed by the defect reaction[40]

$$\frac{1}{2}O_2(g) + 2Mn^{3+} \rightarrow O_i^{2-} + 2Mn^{4+} \quad (1)$$

where an oxygen interstitial O_i^{2-} is formally charge compensated by two holes on the Mn sublattice, such that one O_i^{2-} oxidizes two Mn^{3+} to Mn^{4+}. Recent experimental work on oxygen-loaded hexagonal $RMnO_3$ (R = Ho, Er, and Y)[30] and a recent DFT study of interstitial oxygen in $YMnO_3$[39] indicate that oxygen interstitials occupy the Mn layer, consistent with the Mn ions' ability to change their oxidation state; we study this arrangement here. We performed two structural relaxations starting with the interstitial oxygen at two different symmetry-inequivalent positions in the Mn layer, with the coordinates $(\frac{1}{3}, \frac{1}{3}, \frac{3}{4})$ and $(\frac{2}{3}, \frac{2}{3}, \frac{1}{4})$. Both starting structures relaxed to the ferroelectric $P6_3cm$-type structure of the stoichiometric material. Figure 2a,b shows the location of and structure with the lowest-energy oxygen interstitial, with initial location $(\frac{1}{3}, \frac{1}{3}, \frac{3}{4})$, which we found to be 0.1 meV per formula unit lower in energy than the other oxygen interstitial site; we note that both formation energies are rather low. It can be seen from Figure 2a that the local environment of the oxygen interstitial is perovskite-like with the Mn ions surrounding the interstitial now 6-coordinated with oxygen. The octahedra are strongly distorted, however, with Mn–O

DOI: 10.1021/acs.chemmater.6b04207
Chem. Mater. 2017, 29, 2425–2434

bond lengths in the three octahedra containing the interstitial varying between 1.90 Å and 2.68 Å, 1.87 Å and 2.02 Å, and 1.85 Å and 2.00 Å. Here the smallest bond length in each octahedron is that of the Mn interstitial. The "up−up−down" pattern of In displacements can be seen in Figure 2b; we obtain $\Delta z_1 = 0.001$ and $\Delta z_2 = 0.036$.

The total- and orbital-resolved densities of states for stoichiometric $InMnO_3$ are plotted in Figure 3a and for the lowest-energy structure containing an oxygen interstitial in Figure 3b. We see that the insulating nature is maintained in the oxygen-interstitial containing structure, although the band gap is reduced to ∼0.9 eV. As in the stoichiometric case, the valence band is mainly comprised of Mn d and oxygen p states, and we expect that oxidized $InMnO_{3+\delta}$ will show the same p-type semiconducting behavior observed in Seebeck measurements for the related hexagonal manganite $YMnO_3$.[39] The formal oxidation of Mn to charge compensate oxygen interstitials lifts a fraction of the Mn d-states from below to above the Fermi energy.

Oxygen vacancy formation can formally be expressed by the defect reaction[40]

$$O_O^{2-} + 2Mn^{3+} \rightarrow V_O^{2+} + 2Mn^{2+} + \frac{1}{2}O_2(g) \quad (2)$$

in which an oxygen vacancy V_O^{2+} is formally charge compensated by two electrons donated to the Mn sublattice, with each V_O^{2+} providing two electrons and reducing two Mn^{3+} ions to Mn^{2+}. We calculated the structures and energetics of supercells containing in turn the three symmetry-inequivalent oxygen vacancies—two planar and one apical—for the $P\bar{3}c$-type structure, and the four symmetry-inequivalent oxygen vacancies—two planar and two apical—for the $P6_3cm$-type structure. We find that the lowest energy arrangement has an apical oxygen vacancy and is $P3c1$-type, as shown in Figure 2c,d. This structure was calculated to be 1 meV/f.u. lower in energy than the lowest-energy $P6_3cm$-type structure. Note that the $P3c1$ structure has not been observed as a bulk phase in stoichiometric $InMnO_3$ but was recently reported at the walls separating the partially undistorted antipolar domains in the Ga-doped material.[15] Interestingly, in $YMnO_3$ planar oxygen vacancies are favored compared to apical.[28] This difference may stem from the fact that In is significantly less electropositive than Y (1.78 vs 1.22 on the Pauling scale), resulting in weaker In-apical oxygen than Y-apical oxygen bonds.

The presence of an oxygen vacancy causes significant changes in the density of states, particularly near the Fermi level, as shown in Figure 3c. In particular, an impurity state derived primarily from O p states is formed in the gap, reducing the overall band gap between the top of the valence band and the bottom of the impurity states to ∼0.2 eV. Compared to stoichiometric $InMnO_3$, the Fermi level shifts to above the narrow d_{z^2} orbitals suggesting that $InMnO_{3-\delta}$ would be more likely to show n-type than p-type semiconducting behavior. Similar changes to the electronic structure have been observed experimentally for donor-doped $YMnO_3$.[41]

Indium Vacancies. Indium vacancies can arise from evaporation of In during high-temperature growth or postprocessing or through nonstoichiometry unintentionally introduced during the synthesis process. The corresponding defect reaction depends on whether $InMnO_3$ is present in an oxygen-rich or oxygen-poor environment, with distinctly different charge compensation. In oxygen-rich conditions the formation of one In vacancy is formally charge compensated by oxidation of three Mn ions. This can be expressed as the evaporation of gaseous (g) In from $InMnO_3$

$$InMnO_3 \rightarrow In_{1-\delta}^{3+}Mn_{1-3\delta}^{3+}Mn_{3\delta}^{4+}O_3 + \delta In(g) \quad (3)$$

or as In substoichiometry introduced during synthesis, equivalent to Mn excess, which in Kröger−Vink notation corresponds to the following reaction:

$$\frac{1}{2}Mn_2O_3 + 2Mn_{Mn}^{x} + \frac{3}{4}O_2(g) \xrightarrow{InMnO_3} V_{In}''' + 3Mn_{Mn}^{\bullet} + 3O_O^{x} \quad (4)$$

where V_{In}''' is an In vacancy with a relative charge of −3 and $Mn_{Mn}^{\bullet}$ indicates Mn oxidized to Mn^{4+}. In oxygen-poor conditions, In vacancies are charge compensated by oxygen vacancies:

$$InMnO_3 \rightarrow In_{1-\delta}^{3+}Mn^{3+}O_{3-3\delta/2} + \delta In(g) + \frac{3\delta}{4}O_O^{x} \quad (5)$$

which in Kröger−Vink notation becomes

$$\frac{1}{2}Mn_2O_3 \xrightarrow{InMnO_3} V_{In}''' + Mn_{Mn}^{\times} + \frac{3}{2}V_O^{\bullet\bullet} + \frac{3}{2}O_2(g) \quad (6)$$

Since constructing a cell for DFT calculations of In vacancies under oxygen-poor conditions would involve five vacancies—2 V_{In} and 3 V_O—we choose instead to model an intermediate situation where one V_{In} is charge compensated by one V_O and the oxidation of one Mn ion, which is equivalent to mild hole doping. This situation corresponds to the following reaction:

$$InMnO_3 \rightarrow In_{1-\delta}^{3+}Mn_{1-\delta}^{3+}Mn_{\delta}^{4+}O_{3-\delta} + \delta In(g) + \frac{\delta}{2}O_2(g) \quad (7)$$

which is expressed in Kröger−Vink notation as

$$\frac{1}{2}Mn_2O_3 + \frac{1}{4}O_2(g) \xrightarrow{InMnO_3} V_{In}''' + Mn_{Mn}^{\bullet} + 2O_O^{x} + V_O^{\bullet\bullet} \quad (8)$$

To assess the structural stability upon introduction of In vacancies we perform calculations for both symmetry inequivalent In vacancies and a range of In−O vacancy pairs. As before we construct 2 × 2 × 1 supercells of the trimerized primitive unit cell, giving a stoichiometry of $In_{0.958}MnO_3$ with one In vacancy, and $In_{0.958}MnO_{2.986}$ with an In−O vacancy pair.

For the In-vacancy-only case, we find that the lowest-energy position for an In vacancy is the site around which the trigonal bipyramids tilt away, as shown in Figure 2. The lowest energy structure is polar $P6_3cm$-type. We show the calculated density of states for this structure in Figure 3d as well as the partial charge density plotted in an energy range of 0.3 eV on either side of the Fermi level. Interestingly for a polar structure, the indium vacancy causes the system to become metallic. From the partial charge density we see that the states at the Fermi level consist primarily of oxygen 2p states from the in-plane oxygen atoms directly above and below the In vacancy and the nearest Mn 3d orbitals. This suggests that the charge redistribution caused by the removal of the In atom is confined mostly to the region immediately surrounding the vacancy. Formally, a single In vacancy is charge compensated by three Mn^{4+}, which is equivalent to strong hole doping of $InMnO_3$, resulting in a p-type metal.

To study the In−O vacancy pairs expected to form in less oxygen-rich conditions, we combine the two inequivalent In

DOI: 10.1021/acs.chemmater.6b04207
Chem. Mater. 2017, 29, 2425−2434

sites with three different oxygen sites and calculate the structure and total energy of all six combinations. We find that the lowest-energy structure, shown in Figure 2g,h, is $P6_3cm$-type, although close to the $P3c1$ phase, with the In z coordinates $\Delta z_1 = 0.002$ and $\Delta z_2 = 0.029$. The polar structure is ~6 meV/f.u. lower in energy than the nonpolar $P\bar{3}c$ case. The O vacancy is in the plane, with the In vacancy directly below it; combinations with other O vacancies were all higher in energy. The corresponding density of states is shown in Figure 3e. We see that, as in the case of the In-only vacancy, the In−O vacancy pair induces metallicity. In this case, the states nearest to the Fermi level are mainly of in-plane oxygen character, with additional oxygen and manganese contributions. Since the vacant oxygen is an apical atom, the charge mainly redistributes to the in-plane oxygen states.

In Table 1 we summarize our calculations of the structure types so far. We see that, in each of the defect cases considered, the lowest energy state is polar, suggesting that the presence of In or O point defects is not detrimental to the formation of a polar state. In the case of In vacancies and In−O vacancy complexes, however, the ground state is metallic which will disfavor ferroelectric switching of the polarization due to the associated screening of any applied electric field.

Table 1. Calculated Lattice Parameters and Structure Types for the Lowest-Energy Stoichiometric and Defective $InMnO_3$ Materials[a]

type	space group	a (Å)	c (Å)
stoichiometric	$P6_3cm$	5.94	11.49
O interstitial	$P6_3cm$	5.93	11.50
O vacancy	$P3c1$	5.96	11.48
In vacancy	$P6_3cm$	5.94	11.60
In−O vacancy pair	$P6_3cm$	5.94	11.56

[a]The reported lattice parameters are calculated for 120-atom unit cells with the in-plane lattice parameter, a, divided by 2.

It was established in earlier work[10,15] that the nature of domain formation in hexagonal manganites, in particular the width of domain walls and the concentration of domain wall intersections, is dependent on the details of the energy barrier connecting polar and nonpolar states. In particular, the different polar domains in the $P6_3cm$ ground state are separated by nonpolar ($P\bar{3}c$) domain walls. Conversely, the nonpolar domains in the $P\bar{3}c$ structure have polar domain walls. The pathway between the polar and the nonpolar states corresponds to the variation of tilt angle, ϕ, from 0 to 30°, around the "brim" of the Mexican hat-shaped potential energy surface that characterizes the symmetry-lowering phase transition.[13] To estimate the effect of point defects on this energy path in $InMnO_3$, we calculated the energy difference between the polar $P6_3cm$-type ($\phi = 60°$) and the centrosymmetric $P\bar{3}c$-type ($\phi = 30°$) structures first for the stoichiometric compound and then for the various defect combinations. Consistent with ref 15, for our choice of exchange-correlation functional the $P\bar{3}c$ structure is highest in energy and the polar $P6_3cm$ structure lowest in energy for the stoichiometric compound, with an energy difference of ~4 meV/f.u. This energy difference increases to ~6 meV/f.u. with the inclusion of In−O vacancy pairs. For the other three cases—O interstitials, O vacancies, and In vacancies—both the nonpolar and the polar initialized structures relaxed to polar space groups. This suggests that the inclusion of any defect will tend to stabilize a polar structure adopting either the $P6_3cm$ or the $P3c1$ symmetry.

Ga Substitution. For studies of Ga−Mn alloying we used a supercell containing 6 formula units (30 atoms) and replaced between 0 and 6 Mn atoms with Ga, resulting in Ga concentrations of 0%, 16.67%, 33%, 50%, 66.67%, 83.33%, and 100%. For each concentration of Ga, all symmetry-inequivalent combinations of sites for substitution allowed by the choice of supercell were calculated. We note that the nearest-neighbor in-plane interactions between the Mn spins remain antiferromagnetic, but we expect the overall ordering magnetic ordering temperature to decrease with increasing Ga concentration due to the dilution of the magnetic ions.

Structure. The calculated lowest-energy arrangements of the Mn and Ga ions for each alloy concentration are shown in the top panel of Figure 4 with the relaxed structures shown below. We see an evolution from the $P6_3cm$ structure of $InMnO_3$ through polar $P3c1$- and nonpolar $P\bar{3}c$-types to the high symmetry paraelectric $P6_3/mmc$ structure of $InGaO_3$. The calculated energy differences between the $P6_3cm$-, $P\bar{3}c$-, and $P6_3/mmc$-type structures are given in Table 2.

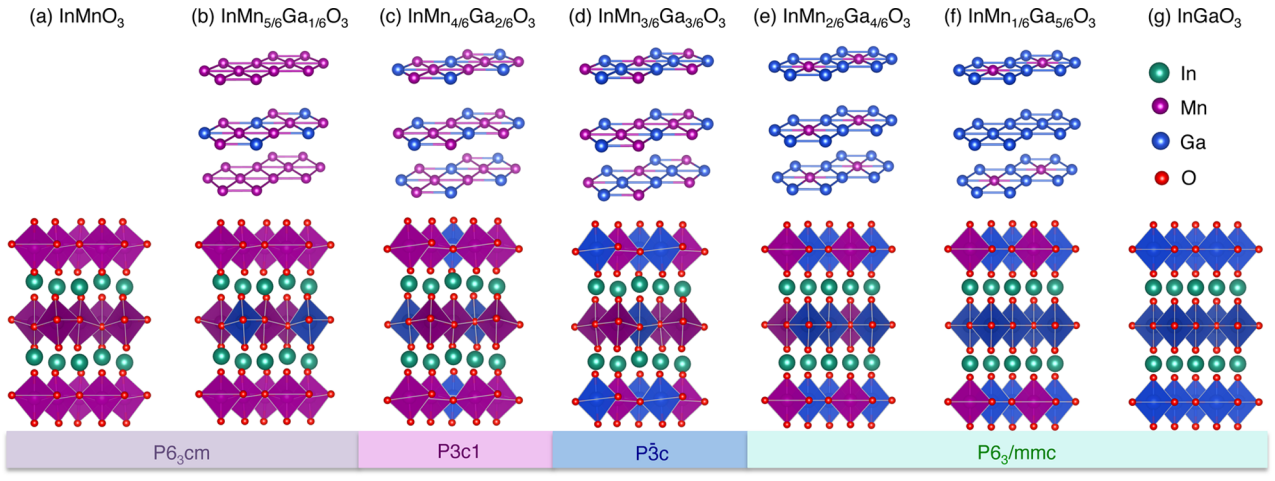

Figure 4. Calculated lowest-energy Mn−Ga orderings (top panel) and structures (lower panel) for $InMn_xGa_{1-x}O_3$. We see an evolution from the polar $P6_3cm$ symmetry of stoichiometric $InMnO_3$ to the paraelectric $P6_3/mmc$ symmetry of $InGaO_3$ via polar $P6_3cm$- and $P3c1$-type to nonpolar $P\bar{3}c$-type and nonpolar $P6_3/mmc$-type as a function of increasing Ga concentration.

DOI: 10.1021/acs.chemmater.6b04207
Chem. Mater. 2017, 29, 2425−2434

Table 2. Calculated Total Energies Relative to That of the $P6_3cm$-Type Structure for the Lowest-Energy (Mn,Ga) Arrangements of $In(Mn,Ga)O_3$[a]

	energy (meV/f.u.)		
Ga fraction	$P6_3cm$	$P\bar{3}c$	$P6_3/mmc$
0	0	4.30	45.88
1/6	0	1.45	30.13
1/3	–	–	15.01
1/2	0	−0.07	5.49
2/3	0	0.02	−0.43
5/6	0	0.37	−0.02
1	0	−0.07	−0.11

[a]The energies shown are per 5 atoms. Note that for 1/3 Ga, both $P6_3cm$- and $P\bar{3}c$-type starting points relaxed to $P3c1$-type symmetry.

With one Ga atom in the unit cell (1/6 Ga), Figure 4(b), the structure retains the polar $P6_3cm$-type structure of stoichiometric $InMnO_3$. The energy difference between the ferroelectric $P6_3cm$-type and nonpolar $P\bar{3}c$-type symmetries is reduced, however, from ∼4 meV/f.u. for stoichiometric $InMnO_3$ to ∼1 meV/f.u. with 1/6 Ga. With two Ga atoms per unit cell (1/3 Ga), we find that the Ga atoms separate as far as possible spatially, and both the $P6_3cm$-type and $P\bar{3}c$-type initialized structures relax to the polar $P3c1$-type structure (Figure 4c). When half of the Mn ions are replaced by Ga, it is lowest energy for two Ga ions to occupy one layer with the third in the second layer (Figure 4d). The resulting structure is nonpolar $P\bar{3}c$-type with the In ions displacing in the "up−none−down" pattern; the $P\bar{3}c$ structure is ∼0.1 meV/f.u. lower in energy than the $P6_3cm$-type. With four Ga atoms in the unit cell, 2/3 Ga, the lowest-energy structure has two Ga atoms in each layer and adopts the high-symmetry $P6_3/mmc$-type structure of the 5/6 substituted composition and of $InGaO_3$ (Figure 4e−g).

Figure 5 shows our calculated lattice parameters for the different Ga fractions. As the percentage of Ga increases, we find that the a lattice parameter decreases from ∼5.89 Å to ∼5.71 Å while the c lattice parameter increases, as expected from the lattice parameters of stoichiometric $InMnO_3$ and $InGaO_3$. This is consistent with experiments on solid solutions of $InMn_{1-x}Ga_xO_3$,[42] which report the in-plane lattice parameter

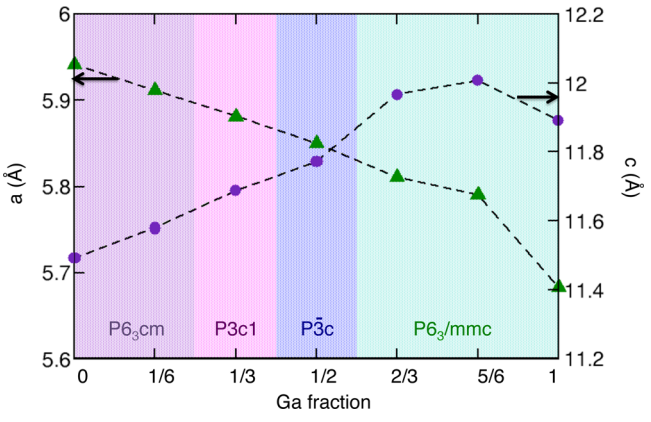

Figure 5. Calculated lattice parameters as a function of Ga concentration for the lowest-energy $In(Mn,Ga)O_3$ alloy structures. The left y-axis shows the in-plane lattice parameter, a, and the right y-axis the out-of-plane lattice parameter, c, both for 30 atom unit cells. The different structure types are indicated.

decreasing with x from ∼5.88 Å to ∼5.73 Å and the out-of-plane lattice parameter increasing from ∼11.50 Å to ∼12.05 Å. The decrease in a lattice parameter is explained by the Shannon−Prewitt radius of five-coordinated Mn^{3+} (0.58 Å) larger than that of Ga^{3+} (0.55 Å).[43] The increase in the out-of-plane lattice parameter is likely due to filling of the d_{z^2} antibonding states with increased Ga content, causing an increase in the apical Mn−O bond length and a reduction in tilting. This effect also contributes to the stabilization of the untilted $P6_3/mmc$ structure for $x \geq 0.6$.

Electronic Structure. The calculated band gaps for the lowest energy structures as a function of Ga content are shown in Figure 6. We see that the materials are insulating for all Ga

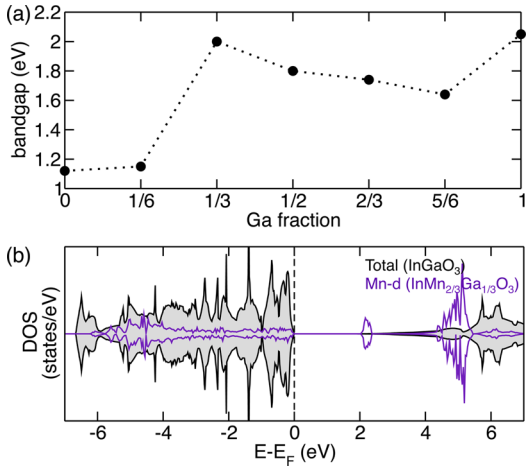

Figure 6. (a) Calculated band gap for the $In(Mn,Ga)O_3$ series as a function of Ga content. The end points (0 and 1 Ga fraction) correspond to the stoichiometric $InMnO_3$ and $InGaO_3$ compounds, respectively. (b) Electronic densities of states calculated for stoichiometric $InGaO_3$ (black line, gray shading) with the Mn-d states of $InMn_{2/3}Ga_{1/3}O_3$ are superimposed in purple.

concentrations, with the band gap increasing from ∼1.1 eV for stoichiometric $InMnO_3$ to 2 eV for stoichiometric $InGaO_3$. In between the end-point compounds the behavior is not monotonic, likely due to the ordered supercells used in our calculations.

The effect of Mn-site alloying on the electronic structure was studied previously for $Y(In,Mn)O_3$,[44] where it was found that materials with substantial In content were a vibrant blue color. This was explained by the combination of the wide band gap of $YInO_3$ and the narrow Mn d_{z^2} crystal field level within the gap, which absorbs with a symmetry-allowed transition in the red region of the spectrum. In Figure 6b we show the calculated density of states of $InGaO_3$ (black line, shaded) with its large 2 eV gap, with the Mn-d states of $InMn_{2/3}Ga_{1/3}O_3$ superimposed in purple. The narrow midgap d band is clearly visible. A previous correlation[44] was noted between the energy of the d_{z^2} states with respect to the top of the valence band and the Mn−O apical bond length, with an optimal value of 1.89 Å for the most intense blue color. In our system, Ga-doping varies this apical bond length between 1.91 Å for $InMnO_3$ to a maximum of 1.97 Å for 1/2 Ga doping, dropping back to 1.90 Å in $InGaO_3$. These similarities suggest the $In(Mn,Ga)O_3$ series as a potential system for exploring new blue chromophores.

DOI: 10.1021/acs.chemmater.6b04207
Chem. Mater. 2017, 29, 2425−2434

DISCUSSION

Our first finding is that the presence of oxygen and indium point defects does not disfavor polar behavior in $InMnO_3$, with most combinations maintaining the $P6_3cm$-type structure of the stochiometric compound, or in the case of oxygen vacancies the lower-symmetry $P3c1$-type. The a and c lattice parameters also change only slightly (less that ∼0.1 Å.) For the In−O vacancy pair, the energy difference between the ferroelectric and paraelectric phases even increases compared with the stoichiometric case from ∼4 meV/f.u. to ∼6 meV/f.u. In contrast, gallium alloying on the manganese site significantly influences the ground state crystal structure, with a polar phase ($P6_3cm$-type and then $P3c1$-type) favored up to a Ga concentration of ∼40%, followed by the low-symmetry nonpolar $P\bar{3}c$-type structure for Ga concentrations of ∼40%−60%, with the high-symmetry, untilted paraelectric $P6_3/mmc$ phase stabilized for higher concentrations. Our calculations are consistent with recent HAADF-TEM studies of $In(Mn,Ga)O_3$.[15]

The evolution of the structure can be rationalized in terms of the change in the lattice parameters caused by substitution of Ga. With increasing Ga concentration, the a lattice parameter smoothly decreases, consistent with the slightly smaller ionic radius of Ga, while c increases, reflecting a reduction in the magnitude of polyhedral tilting and reducing the O 2p−In 5s covalency; this has been previously shown to favor the polar over the nonpolar state.[14] In contrast, $YMn_{1-x}Ga_xO_3$ does not show a structural phase transition, retaining $P6_3cm$ symmetry throughout the entire Ga doping range.[45,46] Note that transitions from hexagonal $P6_3cm$ to perovskite structure have been reported for $YMn_{1-x}Ti_xO_3$ at $x = 0.2$[47,48] and for $YMn_{1-x}Fe_xO_3$ at $x = 0.3$.[49]

The various defects and dopants have pronounced effects on the electronic structure of the material, most notably on the band gap. The density of states with oxygen interstitials and oxygen vacancies remains gapped; however, the band gap is reduced from 1.2 eV to 0.9 eV and 0.2 eV, respectively. For both the indium-only vacancy and the indium−oxygen vacancy pair, the material becomes metallic, with the states at the Fermi level being of O-p character. In the latter cases, the ground state is thus both polar and metallic. Careful control of the point defect population may thus be an alternative to heteroepitaxial engineering[50] for designing polar metals. Our calculations shows that $YMn_{1-x}Ga_xO_3$ is an insulator throughout the whole doping range, with the band gap varying between 1.1 and 2 eV. This variation in band gap—related to the apical Mn−O bond length—could result in interesting optical properties and offers it as a potential alternative for studying new blue pigments in the hexagonal Manganite class.

From an experimental point of view, In vacancies and substitutional Ga are "irreversible defects", meaning that once introduced during synthesis or processing of the materials, they cannot be eliminated or easily created. In contrast, point defects only involving oxygen ions are "reversible defects", meaning that they can be created or removed by carefully controlling the thermal and atmospheric history of a sample. Low temperature and high p_{O_2} will favor oxygen interstitials,[29,30,39] while high temperature and low p_{O_2} will promote oxygen vacancy formation.[40] Oxidizing or reducing $InMnO_{3\pm\delta}$ pushes the intrinsic anti-Frenkel equilibrium $K_F = [V_O^{**}][O_i'']$ toward predominantly vacancies or interstitials. We propose that the strong coupling between defect chemistry and physical properties such as polar versus nonpolar or insulating versus metallic character indicated by our calculations constitutes an avenue of opportunities for manipulating the properties of indium manganite. Studies of other hexagonal manganites show significant oxygen mobility down to 150 to 250 °C, depending on the R^{3+} cation,[29,30] while low temperature topotactic reduction of $YMnO_{3-\delta}$ has been demonstrated at 225 °C. We propose, for example, that In-deficient $In_{1-x}MnO_{3.00}$, which we find to be a polar metal, could be rendered locally insulating by lithography and local topotactic reduction of the oxygen content. A related possibility is to use $In_{1-x}MnO_{3\pm\delta}$ as a memristive material in contact with an oxygen reservoir. Additionally, since semiconducting $InMnO_{3\pm\delta}$ can accommodate both oxygen vacancies and interstitials, the majority charge carriers can easily be tuned to be electrons or holes, respectively. Oxygen defects could therefore be used to reversibly create or remove $p-n$ junctions, which should occur where local gradients in oxygen stoichiometry cross $\delta = 0$.

CONCLUSIONS

We have shown using first-principles calculations that the relative stability of the polar and nonpolar phases of $InMnO_3$ is strongly affected by the introduction of oxygen point defects, indium vacancies, indium−oxygen vacancy pairs, and Ga substitution. Polar phases are favored for all investigated intrinsic point defects. The electronic properties of $InMnO_3$ can be made insulating, metallic, or close to n-type or p-type semiconducting by controlling the point defect population. The In layer corrugation indicates that the polar $P6_3cm$-type structure of the stoichiometric material remains the ground state with the inclusion of oxygen interstitials and with In vacancies and In−O vacancy pairs. Single oxygen vacancies favor the polar low-symmetry $P3c1$-type structure, while the centrosymmetric $P\bar{3}c$-type structure was not stabilized by any of the investigated intrinsic point defects. With increasing Ga concentration in $InMn_{1-x}Ga_xMnO_3$, the structural ground state evolves through the sequence polar $P6_3cm$-type−polar $P3c1$-type−nonpolar $P\bar{3}c$-type−nonpolar $P6_3/mmc$-type. Our results point to the use of point defect chemistry as a handle for designing or modifying the structural properties of complex oxides.

AUTHOR INFORMATION

Corresponding Authors

*(S.M.G.) E-mail: sgriffin@lbl.gov.
*(S.M.S.) E-mail: selbach@ntnu.no.
*(N.A.S.) E-mail: nicola.spaldin@mat.ethz.ch.

ORCID

Sverre M. Selbach: 0000-0001-5838-8632

Notes

The authors declare no competing financial interest.

ACKNOWLEDGMENTS

We thank Sang-Wook Cheong and Fei-Ting Huang for helpful discussions. N.A.S. and S.M.G. were funded by the ETH Zürich and by the ERC Advanced Grant program, No. 291151. This work was supported by a grant from the Swiss National Supercomputing Centre (CSCS) under project ID s624. M.R. and S.M.S. were supported by the Norwegian Metacentre for Computational Science, Uninett Sigma2, through the project NN9264K. S.M.G. acknowledges financial support by the Swiss

DOI: 10.1021/acs.chemmater.6b04207
Chem. Mater. 2017, 29, 2425−2434

National Science Foundation Early Postdoctoral Mobility Program.

REFERENCES

(1) Schmid, H. Multiferroic magnetoelectrics. *Ferroelectrics* **1994**, *162*, 317.
(2) Fiebig, M. Revival of the magnetoelectric effect. *J. Phys. D: Appl. Phys.* **2005**, *38*, R123.
(3) Ascher, E.; Rieder, H.; Schmid, H.; Stössel, H. Some properties of ferromagnetoelectric Nickel-Iodine Boracite, $Ni_3B_7O_{13}I$. *J. Appl. Phys.* **1966**, *37*, 1404−1405.
(4) Khomskii, D. Multiferroics: Different ways to combine magnetism and ferroelectricity. *J. Magn. Magn. Mater.* **2006**, *306*, 1−8.
(5) Spaldin, N. A.; Fiebig, M. The renaissance of magnetoelectric multiferroics. *Science* **2005**, *309*, 391−392.
(6) Hill, N. A. Why are there so few magnetic ferroelectrics? *J. Phys. Chem. B* **2000**, *104*, 6694−6709.
(7) Lorenz, B. Hexagonal Manganites - ($RMnO_3$): Class (I) Multiferroics with Strong Coupling of Magnetism and Ferroelectricity. *ISRN Condens. Matter Phys.* **2013**, *2013*, 497073.
(8) Meier, D.; Seidel, J.; Cano, A.; Delaney, K.; Kumagai, Y.; Mostovoy, M.; Spaldin, N. A.; Ramesh, R.; Fiebig, M. Anisotropic conductance at improper ferroelectric domain walls. *Nat. Mater.* **2012**, *11*, 284.
(9) Becher, C.; Maurel, L.; Aschauer, U.; Lilienblum, M.; Magén, C.; Meier, D.; Langenberg, E.; Trassin, M.; Blasco, J.; Krug, I. P.; Algarabel, P. A.; Spaldin, N. A.; Pardo, J. A.; Fiebig, M. Strain-induced coupling of electrical polarization and structural defects in $SrMnO_3$ films. *Nat. Nanotechnol.* **2015**, *10*, 661−665.
(10) Griffin, S.; Lilienblum, M.; Delaney, K.; Kumagai, Y.; Fiebig, M.; Spaldin, N. Scaling behavior and beyond equilibrium in the hexagonal manganites. *Phys. Rev. X* **2012**, *2*, 041022.
(11) van Aken, B. B.; Palstra, T. T. M.; Filippetti, A.; Spaldin, N. A. The origin of ferroelectricity in magnetoelectric $YMnO_3$. *Nat. Mater.* **2004**, *3*, 164−170.
(12) Fennie, C. J.; Rabe, K. M. Ferroelectric transition in $YMnO_3$ from first principles. *Phys. Rev. B: Condens. Matter Mater. Phys.* **2005**, *72*, 100103.
(13) Artyukhin, S.; Delaney, K. T.; Spaldin, N. A.; Mostovoy, M. Landau theory of topological defects in multiferroic hexagonal manganites. *Nat. Mater.* **2014**, *13*, 42−49.
(14) Kumagai, Y.; Belik, A. A.; Lilienblum, M.; Leo, N.; Fiebig, M.; Spaldin, N. A. Observation of persistent centrosymmetricity in the hexagonal Manganite family. *Phys. Rev. B: Condens. Matter Mater. Phys.* **2012**, *85*, 174422.
(15) Huang, F.-T.; Wang, X.; Griffin, S. M.; Kumagai, Y.; Gindele, O.; Chu, M.-W.; Horibe, Y.; Spaldin, N. A.; Cheong, S.-W. Duality of Topological Defects in Hexagonal Manganites. *Phys. Rev. Lett.* **2014**, *113*, 267602.
(16) Giaquinta, D. M.; Zur Loye, H. C. Indium manganese trioxide: a new transition metal oxide with an unusual ABO_3 structure. *J. Am. Chem. Soc.* **1992**, *114*, 10952−10953.
(17) Greedan, J.; Bieringer, M.; Britten, J.; Giaquinta, D.; zur Loye, H.-C. Synthesis, crystal structure, and unusual magnetic properties of $InMnO_3$. *J. Solid State Chem.* **1995**, *116*, 118−130.
(18) Serrao, C. R.; Krupanidhi, S.; Bhattacharjee, J.; Waghmare, U. V.; Kundu, A. K.; Rao, C. $InMnO_3$: A biferroic. *J. Appl. Phys.* **2006**, *100*, 076104−076104.
(19) Belik, A. A.; Kamba, S.; Savinov, M.; Nuzhnyy, D.; Tachibana, M.; Takayama-Muromachi, E.; Goian, V. Magnetic and dielectric properties of hexagonal $InMnO_3$. *Phys. Rev. B: Condens. Matter Mater. Phys.* **2009**, *79*, 054411.
(20) Rusakov, D. A.; Belik, A. A.; Kamba, S.; Savinov, M.; Nuzhnyy, D.; Kolodiazhnyi, T.; Yamaura, K.; Takayama-Muromachi, E.; Borodavka, F.; Kroupa, J. Structural evolution and properties of solid solutions of hexagonal $InMnO_3$ and $InGaO_3$. *Inorg. Chem.* **2011**, *50*, 3559−3566.
(21) Bekheet, M. F.; Svoboda, I.; Liu, N.; Bayarjargal, L.; Irran, E.; Dietz, C.; Stark, R. W.; Riedel, R.; Gurlo, A. Ferroelectric $InMnO_3$: Growth of single crystals, structure and high-temperature phase transitions. *J. Solid State Chem.* **2016**, *241*, 54−63.
(22) Yu, T.; Gao, P.; Wu, T.; Tyson, T.; Lalancette, R. Ferroelectricity in single crystal $InMnO_3$. *Appl. Phys. Lett.* **2013**, *102*, 172901.
(23) Huang, F.-T.; Wang, X.; Oh, Y.; Kurushima, K.; Mori, S.; Horibe, Y.; Cheong, S.-W. Delicate balance between ferroelectricity and antiferroelectricity in hexagonal $InMnO_3$. *Phys. Rev. B: Condens. Matter Mater. Phys.* **2013**, *87*, 184109.
(24) Kalinin, S. V.; Borisevich, A.; Fong, D. Beyond condensed matter physics on the nanoscale: the role of ionic and electrochemical phenomena in the physical functionalities of oxide materials. *ACS Nano* **2012**, *6*, 10423−10437.
(25) Kalinin, S. V.; Spaldin, N. A. Functional ion defects in transition metal oxides. *Science* **2013**, *341*, 858−859.
(26) Aschauer, U.; Pfenninger, R.; Selbach, S. M.; Grande, T.; Spaldin, N. A. Strain-controlled oxygen vacancy formation and ordering in $CaMnO_3$. *Phys. Rev. B: Condens. Matter Mater. Phys.* **2013**, *88*, 054111.
(27) Marthinsen, A.; Faber, C.; Aschauer, U.; Spaldin, N. A.; Selbach, S. M. Coupling and competition between ferroelectricity, magnetism, strain, and oxygen vacancies in $AMnO_3$ perovskites. *MRS Commun.* **2016**, *6*, 182.
(28) Overton, A. J.; Best, J. L.; Saratovsky, I.; Hayward, M. A. Influence of Topotactic Reduction on the Structure and Magnetism of the Multiferroic $YMnO_3$. *Chem. Mater.* **2009**, *21*, 4940−4948.
(29) Remsen, S.; Dabrowski, B. Synthesis and Oxygen Storage Capacities of Hexagonal $Dy_{1-x}Y_xMnO_{3+\delta}$. *Chem. Mater.* **2011**, *23*, 3818−3827.
(30) Abughayada, C.; Dabrowski, B.; Kolesnik, S.; Brown, D. E.; Chmaissem, O. Characterization of Oxygen Storage and Structural Properties of Oxygen-Loaded Hexagonal $RMnO_{3+\delta}$ (R = Ho, Er, and Y). *Chem. Mater.* **2015**, *27*, 6259−6267.
(31) Gélard, I.; Jehanathan, N.; Roussel, H.; Gariglio, S.; Lebedev, O. I.; Van Tendeloo, G.; Dubourdieu, C. Off-Stoichiometry Effects on the Crystalline and Defect Structure of Hexagonal Manganite $REMnO_3$ Films (RE = Y, Er, Dy). *Chem. Mater.* **2011**, *23*, 1232−1238.
(32) Lide, D. R. *CRC Handbook of Chemistry and Physics*; CRC Press: 2004; Vol. *85*.
(33) Kresse, G.; Furthmüller, J. Efficient iterative schemes for *ab initio* total-energy calculations using a plane-wave basis set. *Phys. Rev. B: Condens. Matter Mater. Phys.* **1996**, *54*, 11169−11186.
(34) Kresse, G.; Hafner, J. Ab initio molecular dynamics for liquid metals. *Phys. Rev. B: Condens. Matter Mater. Phys.* **1993**, *48*, 13115.
(35) Medvedeva, J. E.; Anisimov, V. I.; Korotin, M. A.; Mryasov, O. N.; Freeman, A. J. The effect of Coulomb correlation and magnetic ordering on the electronic structure of two hexagonal phases of ferroelectromagnetic $YMnO_3$. *J. Phys.: Condens. Matter* **2000**, *12*, 4947−4958.
(36) Perdew, J. P.; Burke, K.; Ernzerhof, M. Generalized Gradient Approximation Made Simple. *Phys. Rev. Lett.* **1996**, *77*, 3865−3868.
(37) Perdew, J. P.; Ruzsinszky, A.; Csonka, G. I.; Vydrov, O. A.; Scuseria, G. E.; Constantin, L. A.; Zhou, X.; Burke, K. Restoring the Density-Gradient Expansion for Exchange in Solids and Surfaces. *Phys. Rev. Lett.* **2008**, *100*, 136406.
(38) Dudarev, S. L.; Botton, G. A.; Savrasov, S. Y.; Humphreys, C. J.; Sutton, A. P. Electron-energy-loss spectra and the structural stability of nickel oxide: An LSDA+U study. *Phys. Rev. B: Condens. Matter Mater. Phys.* **1998**, *57*, 1505−1509.
(39) Skjærvø, S. H.; Wefring, E. T.; Nesdal, S. K.; Gaukas, N. H.; Olsen, G. H.; Glaum, J.; Tybell, T.; Selbach, S. M. Interstitial oxygen as a source of p-type conductivity in hexagonal manganites. *Nat. Commun.* **2016**, *7*, 13745.
(40) Selbach, S. M.; Løvik, A. N.; Bergum, K.; Tolchard, J. R.; Einarsrud, M.-A.; Grande, T. Crystal structure, chemical expansion and phase stability of $HoMnO_3$ at high temperature. *J. Solid State Chem.* **2012**, *196*, 528−535.

DOI: 10.1021/acs.chemmater.6b04207
Chem. Mater. 2017, 29, 2425−2434

(41) Van Aken, B. B.; Bos, J.-W. G.; de Groot, R. A.; Palstra, T. T. M. Asymmetry of electron and hole doping in $YMnO_3$. *Phys. Rev. B: Condens. Matter Mater. Phys.* **2001**, *63*, 125127.
(42) Rusakov, D. A.; Belik, A. A.; Kamba, S.; Savinov, M.; Nuzhnyy, D.; Kolodiazhnyi, T.; Yamaura, K.; Takayama-Muromachi, E.; Borodavka, F.; Kroupa, J. Structural evolution and properties of solid solutions of hexagonal $InMnO_3$ and $InGaO_3$. *Inorg. Chem.* **2011**, *50*, 3559−3566.
(43) Shannon, R. D.; Prewitt, C. T. Revised effective ionic radii and systematic studies of interatomic distances in halides and chalcogenides. *Acta Crystallogr., Sect. A: Cryst. Phys., Diffr., Theor. Gen. Crystallogr.* **1976**, *32*, 751−767.
(44) Smith, A. E.; Mizoguchi, H.; Delaney, K.; Spaldin, N. A.; Sleight, A. W.; Subramanian, M. A. Mn^{3+} in Trigonal Bipyramidal Coordination: A New Blue Chromophore. *J. Am. Chem. Soc.* **2009**, *131*, 17084−17086.
(45) Adem, U.; Nugroho, A. A.; Meetsma, A.; Palstra, T. T. M. Ferroelectric displacements in multiferroic $Y(Mn, Ga)O_3$. *Phys. Rev. B: Condens. Matter Mater. Phys.* **2007**, *75*, 014108.
(46) Nugroho, A. A.; Bellido, N.; Adem, U.; Nénert, G.; Simon, C.; Tjia, M. O.; Mostovoy, M.; Palstra, T. T. M. Enhancing the magnetoelectric coupling in $YMnO_3$ by Ga doping. *Phys. Rev. B: Condens. Matter Mater. Phys.* **2007**, *75*, 174435.
(47) Asaka, T.; Nemoto, K.; Kimoto, K.; Arima, T.; Matsui, Y. Crystallographic superstructure of Ti-doped hexagonal $YMnO_3$. *Phys. Rev. B: Condens. Matter Mater. Phys.* **2005**, *71*, 014114.
(48) Mori, S.; Tokunaga, J.; Horibe, Y.; Aikawa, Y.; Katsufuji, T. Magnetocapacitance effect and related microstrucuture in Ti-doped $YMnO_3$. *Phys. Rev. B: Condens. Matter Mater. Phys.* **2005**, *72*, 224434.
(49) Samal, S.; Green, W.; Lofland, S.; Ramanujachary, K.; Das, D.; Ganguli, A. Study on the solid solution of $YMn_{1-x}Fe_xO_3$: Structural, magnetic and dielectric properties. *J. Solid State Chem.* **2008**, *181*, 61−66.
(50) Kim, T. H.; et al. Polar metals by geometric design. *Nature* **2016**, *533*, 68−72.

DOI: 10.1021/acs.chemmater.6b04207
Chem. Mater. 2017, 29, 2425−2434